Electronic Supplementary Material (ESI) for Materials Chemistry Frontiers.

Supporting Information

Large-Scale Deep-Blue Tetraphenylbenzene–Bridged Hybridized Local and Charge Transfer Fluorophore Exhibiting Small Efficiency Roll-Off and Low Amplified Spontaneous Emission Threshold

Shian Ying[a,b], Jichen Lv[a], Yuanzhao Li[b], Yumiao Huo[c], Yuchao Liu[a], Dongge Ma[b], Ling Peng[a] and Shouke Yan[a,d]**

[a] Key Laboratory of Rubber-Plastics, Ministry of Education, Qingdao University of Science and Technology, Qingdao 266042, P. R. China.

[b] Institute of Polymer Optoelectronic Materials and Devices, State Key Laboratory of Luminescent Materials and Devices, South China University of Technology, Guangzhou 510640, P. R. China.

[c] College of Materials Science and Engineering, Shandong University of Science and Technology, Qingdao 266590, P. R. China.

[d] State Key Laboratory of Chemical Resource Engineering, College of Materials Science and Engineering, Beijing University of Chemical Technology, Beijing 100029, P. R. China.

*Corresponding author: pengling615@163.com; skyan@mail.buct.edu.cn

Experimental Methods

1. Experimental measurements

^{1}H NMR and ^{13}C NMR spectra were performed on a Bruker AC500 and AC400 spectrometer via using $CDCl_3$ as the solvent and tetramethylsilane (TMS) as the internal standard respectively. Mass spectra of the target compound was carried out by High Resolution Quadrupole Time of Flight Tandem Mass Spectrometer (TOF-MS). UV-visible absorption spectra and photoluminescence (PL) spectra were measured by Hitachi U-4100 absorption spectrometer and Hitachi F-4600 spectrophoto-meter, respectively. PLQYs were tested using in an integration sphere setup (Hamamatsu C11347-11) equipped with a xenon high-pressure lamp and a multichannel analyzer from 200 to 950 nm. The low temperature fluorescence and phosphorescence spectra were measured in dichloromethane after delay time of 0 and 1 ms on an Edinburgh FLS-980 with an EPL-340 optical laser at 77 K. Thermogravimetric analysis (TGA) of the target compound was determined on a Netzsch (209F1) thermogravimetric analyzer under a nitrogen atmosphere (50 mL min^{-1}) at a heating rate of 10 ^{o}C min^{-1}. Differential scanning calorimetry (DSC) curve was recorded on a Netzsch DSC (204F1) instrument at a heating (or cooling) rate of 10 ^{o}C min^{-1}. HOMO energy level of the target compound was measured on a CHI760D electrochemical workstation via using cyclic voltammetry (CV) with a glass carbon disk as the working electrode, a platinum wire as the counter electrode, a Ag/Ag^{+} (0.01 M of $AgNO_3$ in acetonitrile) as the reference electrode, and ferrocene as the standard reference. The material was dissolved in anhydrous dichloromethane solution with 0.1 mol L^{-1} Bu4NPF6 as the electrolyte to measure the oxidation, from which the HOMO energy level was estimated, whereas LUMO energy level was calculated from the difference between the HOMO energy level and optical bandgap (E_g) which was estimated from onsets of the UV-Vis spectrum in dichloromethane. The atomic force microscopy (AFM) images were conducted with a Bruker Dimension Icon operated under a tapping model with the resonance frequency of 300 kHz and the spring constant of ~26 N/m.

2. Device fabrication and measurement

Patterned indium-tin-oxide (ITO) glasses with a sheet resistance of 20 Ω per square were ultrasonically treated in detergents and deionized water, then dried at 120 °C. After treated by oxygen plasma, ITO-substrates were transferred into the vacuum deposition system. The devices were fabricated under the pressure of $< 2 \times 10^{-4}$ Pa. The evaporation rates were detected by a frequency counter and calibrated by a Dektak 6 M profiler (Veeco). Organic materials, lithium fluoride (LiF) and aluminum (Al) were thermally evaporated at the rates of 1-1.5, 0.2 and 5-10 Å s^{-1} via a shadow mask. The emitting region of devices was 3×3 mm^2 that determined by the overlap between ITO and Al electrodes. The current density–luminance–voltage characteristics of devices were recorded by a constant source of Keithley 2450 source meter and LS160 luminance meter. EL spectra were recorded by using an optical analyzer FlAME-S-VIS-NIR photometer. Supposing the light emitted by OLEDs is in accord with the Lambertian distribution, the EQEs can be estimated from the EL spectra, luminance, and current density.

3. Theoretical calculations

All the density functional theory (DFT) and time dependent DFT (TDDFT) calculations were carried out using Gaussian 09 package. The optimized ground-state geometries, energy levels, and frontier molecular orbital (FMO) distributions were calculated on the basis of DFT by using RB3LYP/6-31G(d, p) method. According to the TDDFT calculation, the optimized excited-state geometries, natural transition orbitals (NTOs), singlet and triplet state energies, and oscillator strength were carried out based on RB3LYP/6-31G(d, p) method. The molecular orbital transitions of $S_0 \rightarrow S_1$ excitation were calculated by Multiwfn 3.3.8. [1]

4. Thin film preparation and ASE measurement

Thin films for ASE measurements were fabricated on the quartz substrates that were cleaned with detergents and deionized water and treated by the UV-ozone. Neat Film and doped films (2, 4, 6, 8 and 10-wt%-doped) in the host material 1,3-bis(carbazol-9-yl)benzene (mCP) were spin-coated from 20 mg mL^{-1} chloroform solutions at a rotational speed of 2000 rpm for 60 s at room temperature and then annealed at 60 °C for 10 mins, corresponding to the thicknesses of 120-160 nm. The ASE properties of the films were performed by optically pumping the samples with the randomly polarized nitrogen laser (repetition rate: 18 Hz) at an excited wavelength of 343 nm. The samples were prepared by cutting the quartz substrates, and the light emission was detected from the edge of the sample. The excitation beam was focused into a stripe with the dimensions of 0.43 × 0.1 cm^2. The ASE threshold of films was determined from the non-linear changes of the emission intensity plotted against the excitation light intensity.

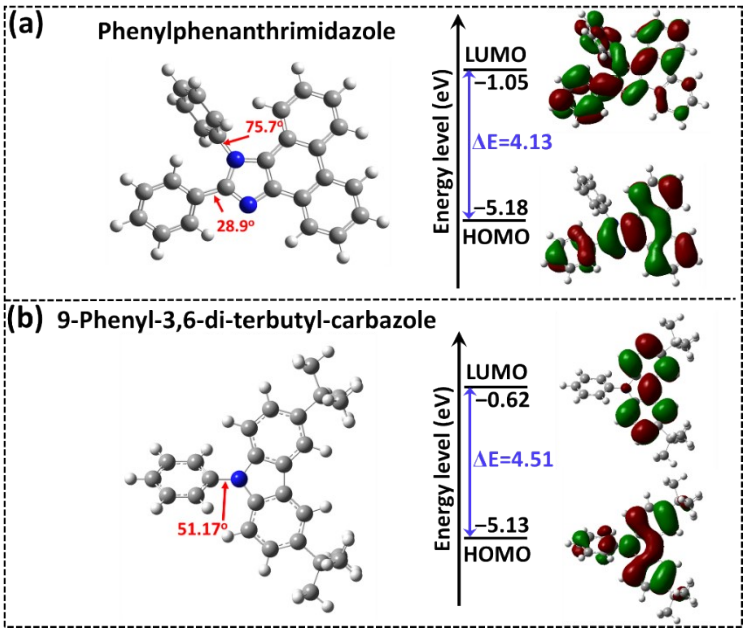

Fig. S1 Calculated energy levels, molecular orbitals, and optimized configurations of phenylphenanthrimidazole and 9-phenyl-3,6-di-terbutyl-carbazole.

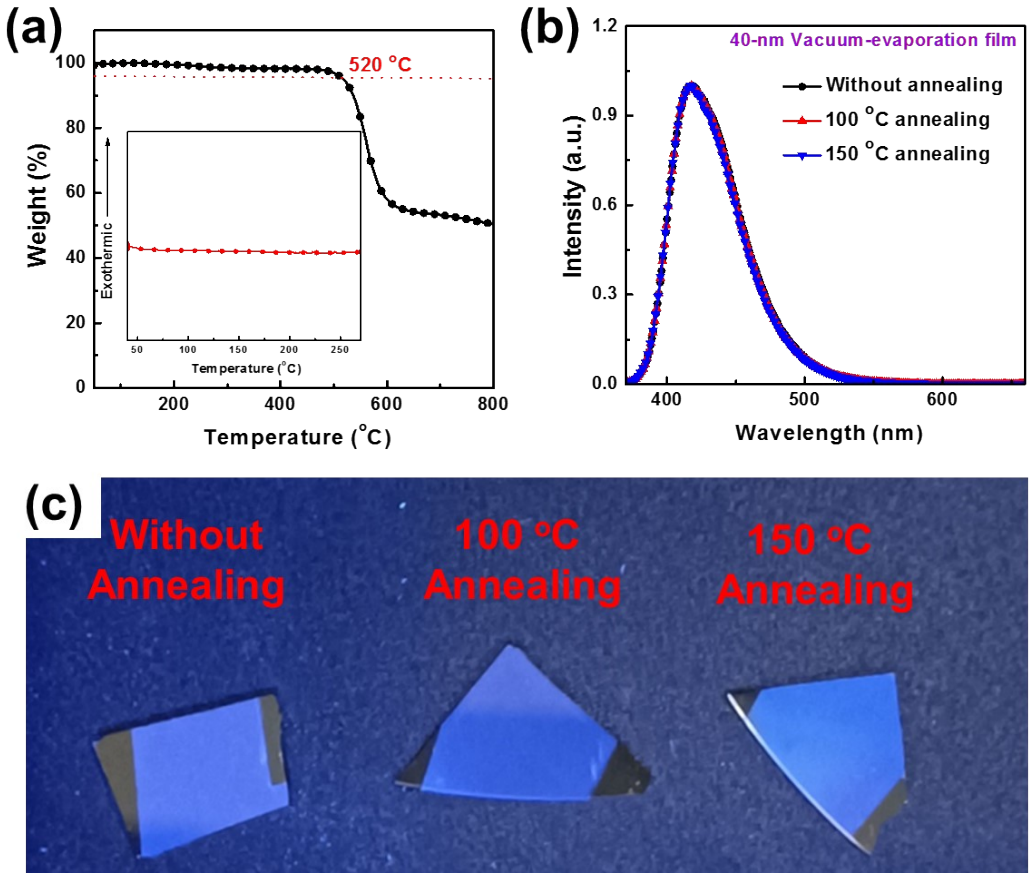

Fig. S2 (a) Thermogravimetric analysis (TGA) and differential scanning calorimetry (DSC) curves of **PTPC**. (b) PL spectra of 40-nm vacuum-evaporation films without/with annealing at 100 and 150 °C for 24 h. (c) Fluorescence images of 40-nm vacuum-evaporation films on silicon wafer at different annealing temperature under 365 nm UV light.

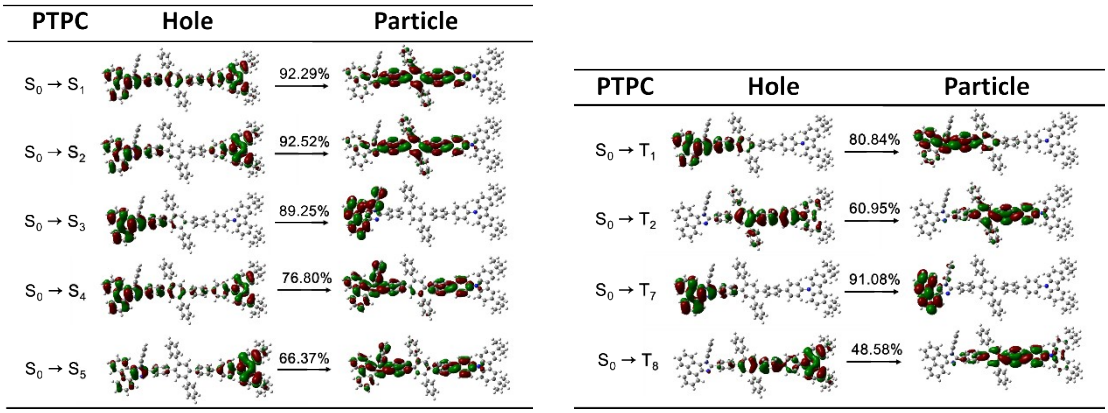

Fig. S3 The calculated NTO distributions of singlet and triplet states of **PTPC**.

Table S1. Energy levels of singlet and triplet states and oscillator strengths of singlet states in **PTPC**.

Excited States	S energy level (eV)	T energy level (eV)	S Oscillator Strength
1	3.3362	2.6252	1.3043
2	3.4329	2.8586	0.0388
3	3.7154	3.0116	0.0095
4	3.7607	3.1552	0.0061
5	3.7844	3.16	0.1792
6	3.8731	3.2232	0.1316
7	3.8956	3.3347	0.1827
8	3.9296	3.4735	0.0988
9	3.9467	3.5065	0.0181
10	3.9622	3.5987	0.0001

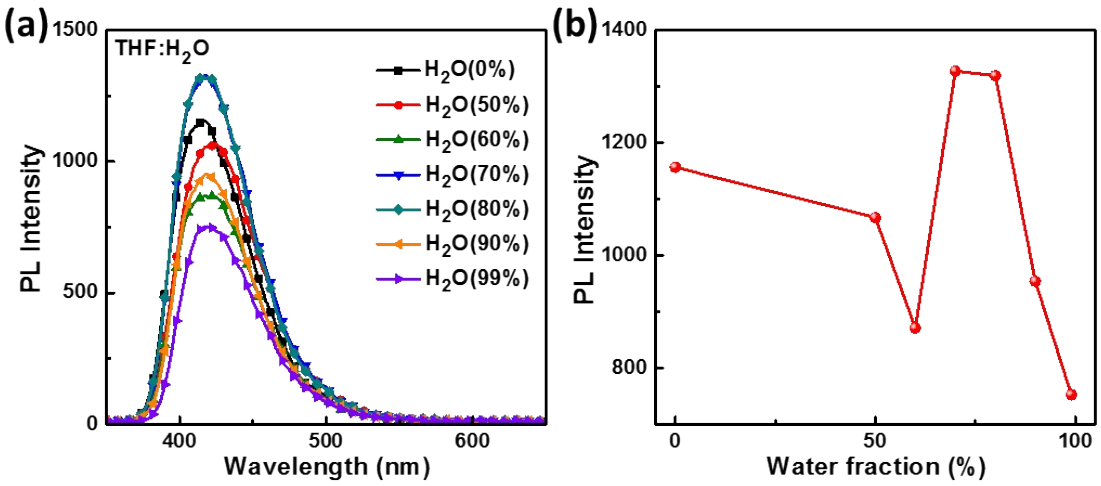

Fig. S4 (a) The PL spectra of **PTPC** in THF/water mixtures with different water fractions. (b) The maximum PL intensity-water fraction curve.

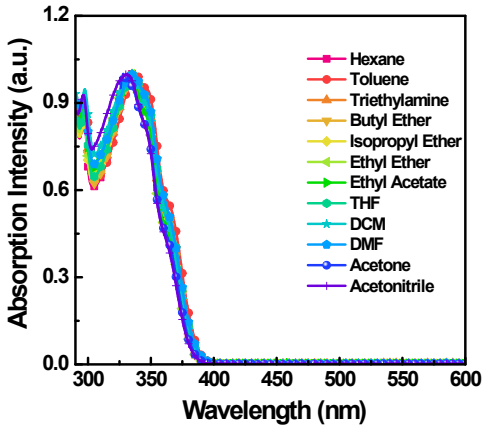

Fig. S5 The UV-vis absorption spectra of **PTPC** in different solvents with the concentration of 1×10^{-5} mol L^{-1}.

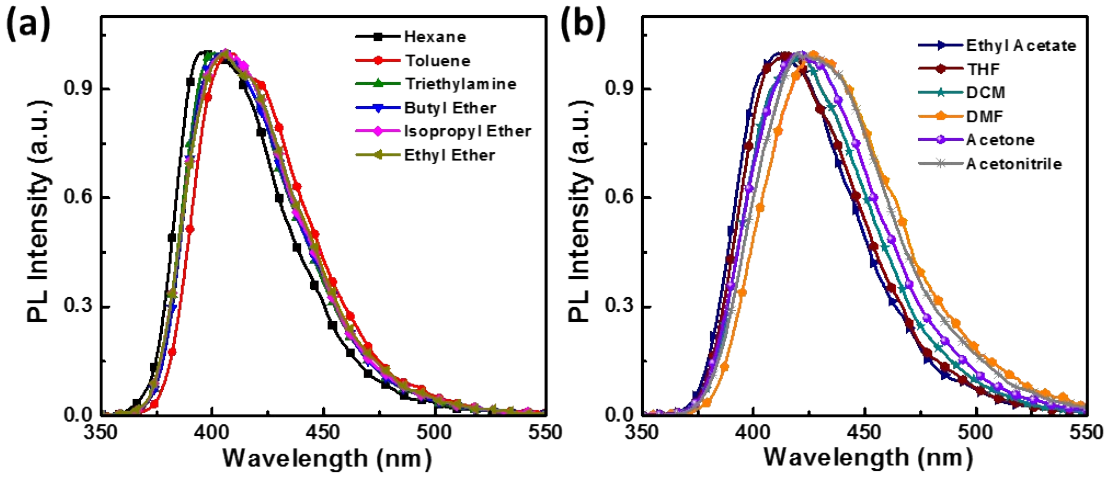

Fig. S6 (a) and (b) The PL spectra of **PTPC** in different solvents with the concentration of 1×10^{-5} mol L^{-1}.

Lippert-Mataga Calculation

The Lippert-Mataga model is calculated by Equation 1 as below.

$$hc(\nu_a - \nu_f) = hc\left(\nu_a^0 - \nu_f^0\right) + \frac{2(\mu_e - \mu_g)^2}{a_0^3} f(\varepsilon,n) \quad (1)$$

$$f(\varepsilon,n) = \frac{\varepsilon - 1}{2\varepsilon + 1} + \frac{n^2 - 1}{2n^2 + 1} \quad (2)$$

$$a_0 = \left(\frac{3M}{4\pi Nd}\right)^{1/3} \quad (3)$$

Where h is the Plank constant, c is the light speed in vacuum, μ_g is the ground-state dipole moment; μ_e is the excited-state dipole moment, $f(\varepsilon, n)$ is the orientational polarizability of solvents, a_0 is the Onsager cavity radius, $\nu_a^0 - \nu_f^0$ is the Stokes shifts when f is zero, respectively. In Equation 2, ε and n are dielectric constant and refractive index of solvent. In Equation 3, N is Avogadro's number, M is molar mass, and d is density of the solvents, respectively.

Take differential on both sides of the Equation 1, the Equation 4 can be obtained:

$$\mu_e = \mu_g + \left\{\frac{hca_0^3}{2} \times \left[\frac{d(\nu_a - \nu_f)}{df(\varepsilon,n)}\right]\right\}^{1/2} \quad (4)$$

The μ_g of **PTPC** (3.75 D) was estimated with the Gaussian 09 package at the level of RB3LYP/6-31G(d, p). a_0 can be estimated by the Equation 3. The $\frac{d(\nu_a - \nu_f)}{df(\varepsilon,n)}$ can be estimated with the solvatochromic experiment data listed in Table S2. With the information above, μ_e can be figured out as mentioned in the manuscript. As a result, a linear relationship with the slope of 6141 (Correlation = 0.967) was achieved, corresponding to the μ_e of 15.77 D.

Table S2. The detailed absorption and emission data of **PTPC** in different solvents.

Solvents	ε	n	f(ε, n)	PTPC		
				λ_a [nm]	λ_f [nm]	ν_a-ν_f [cm^{-1}]
Hexane	1.9	1.375	0.0012	335	396	4598.221016
Toluene	2.38	1.494	0.014	337	407	5103.565934
Triethylamine	2.42	1.401	0.048	336	401	4824.248902
Butyl ether	3.08	1.399	0.096	337	405	4982.23248
Isopropyl ether	3.88	1.368	0.145	335	405	5159.388244
Ethyl ether	4.34	1.352	0.167	335	406	5220.204397
Ethyl acetate	6.02	1.372	0.2	334	411	5609.219517
Tetrahydrofuran	7.58	1.407	0.21	335	416	5812.28473
Dichloromethane	8.93	1.424	0.217	336	422	6065.222297
Dimethylformamide	37	1.427	0.276	336	426	6287.726358
Acetone	20.7	1.359	0.284	334	421	6187.150639
Acetonitrile	37.5	1.344	0.305	331	420	6401.956553

Table S3. The thermal, photophysical and electrochemical parameters of **PTPC**.

	λ_{PL} [nm]	Φ_{PL} [%]	τ [ns]	k_r [h] [$\times 10^8$ s^{-1}]	k_{nr} [i] [$\times 10^8$ s^{-1}]	E_S/E_T [c] [eV]	E_g [f] [eV]	T_d/T_g [j] [eV]	HOMO/LUMO [g] [eV]
	Solution[a]/film[b]								
PTPC	422 [d]/ 430	92.1 [e]/ 82.7	0.917 [e]/ 0.988	10.04/ 8.37	0.87/ 1.75	3.04/ 2.48	3.20	520/ -	-5.41/ -2.21

[a] Measured in dilute solution at room temperature (10^{-5} M); [b] Measured in neat film at room temperature; [c] Singlet (E_S) and triplet (E_T) energies were determined from the highest energy peak of fluorescence and phosphorescence spectra measured in dichloromethane solution at 77 K, respectively; [d] In dilute CH_2Cl_2 solution; [e] In dilute toluene solution; [f] Optical energy bandgap (E_g) is estimated from the onset of the absorption spectra in CH_2Cl_2 solution at room temperature; [g] Measured by cyclic voltammetry where $E_{HOMO} = -4.8 - (E_{ox} - E_{Fc})$, $E_{LUMO} = E_{HOMO} + E_g$; [h] $k_r = \Phi_{PL}/\tau$; [i] $k_{nr} = 1/\tau - k_r$; [j] T_d: Decomposition temperature at 5% weight loss, T_g: Glass transition temperature.

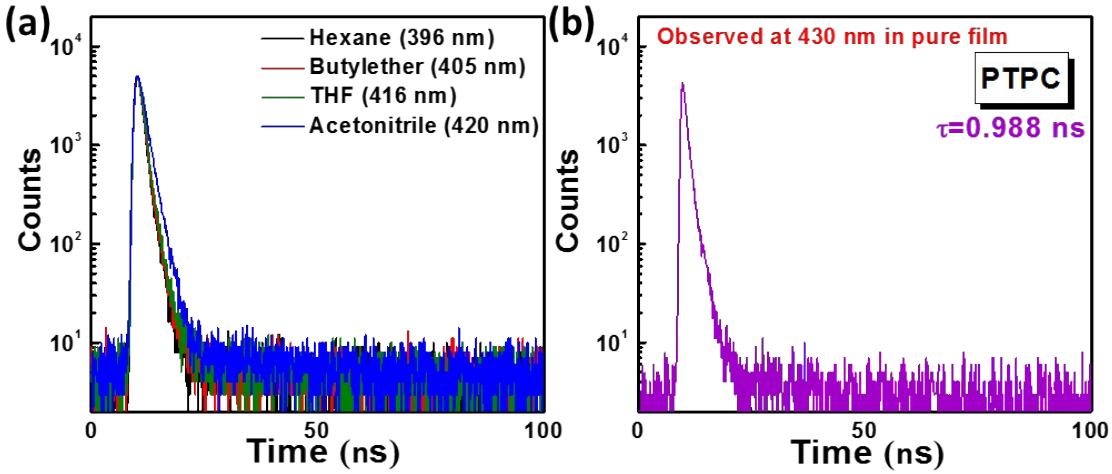

Fig. S7 (a) Transient PL decay curves of **PTPC** in different solvents (hexane, butylether, THF, and acetonitrile) under the excitation of 280 nm. (b) Transient PL decay curve of **PTPC** in neat film under the excitation of 280 nm.

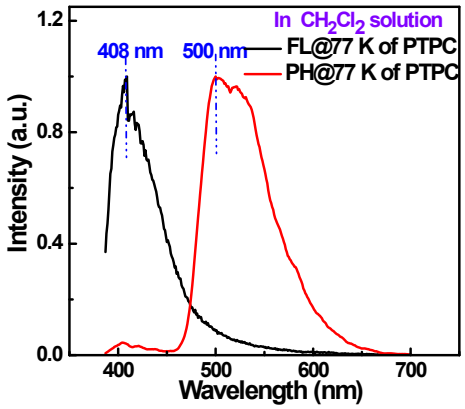

Fig. S8 Low temperature fluorescent and phosphorescent spectra of **PTPC** in CH_2Cl_2 solution at 77 K.

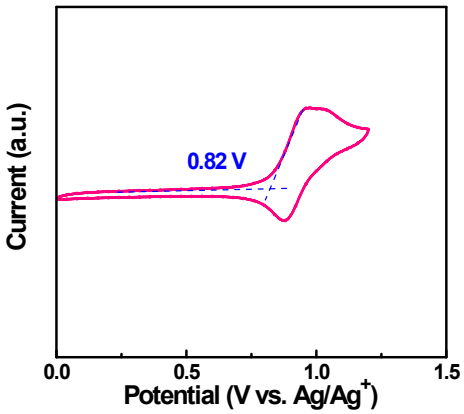

Fig. S9 Cyclic voltammograms curves of **PTPC**.

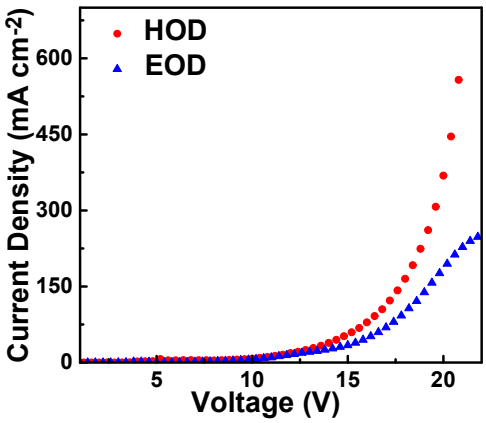

Fig. S10 Current density–voltage plots of hole-only device (HOD) and electron-only device (EOD) with thedevice structures of ITO/ HATCN (20 nm)/ **PTPC** (80 nm)/ HATCN (20 nm)/Al (150 nm) and ITO/ TPBi (10 nm)/ PTPC (80 nm)/ LiF (1 nm)/ Al (150 nm).

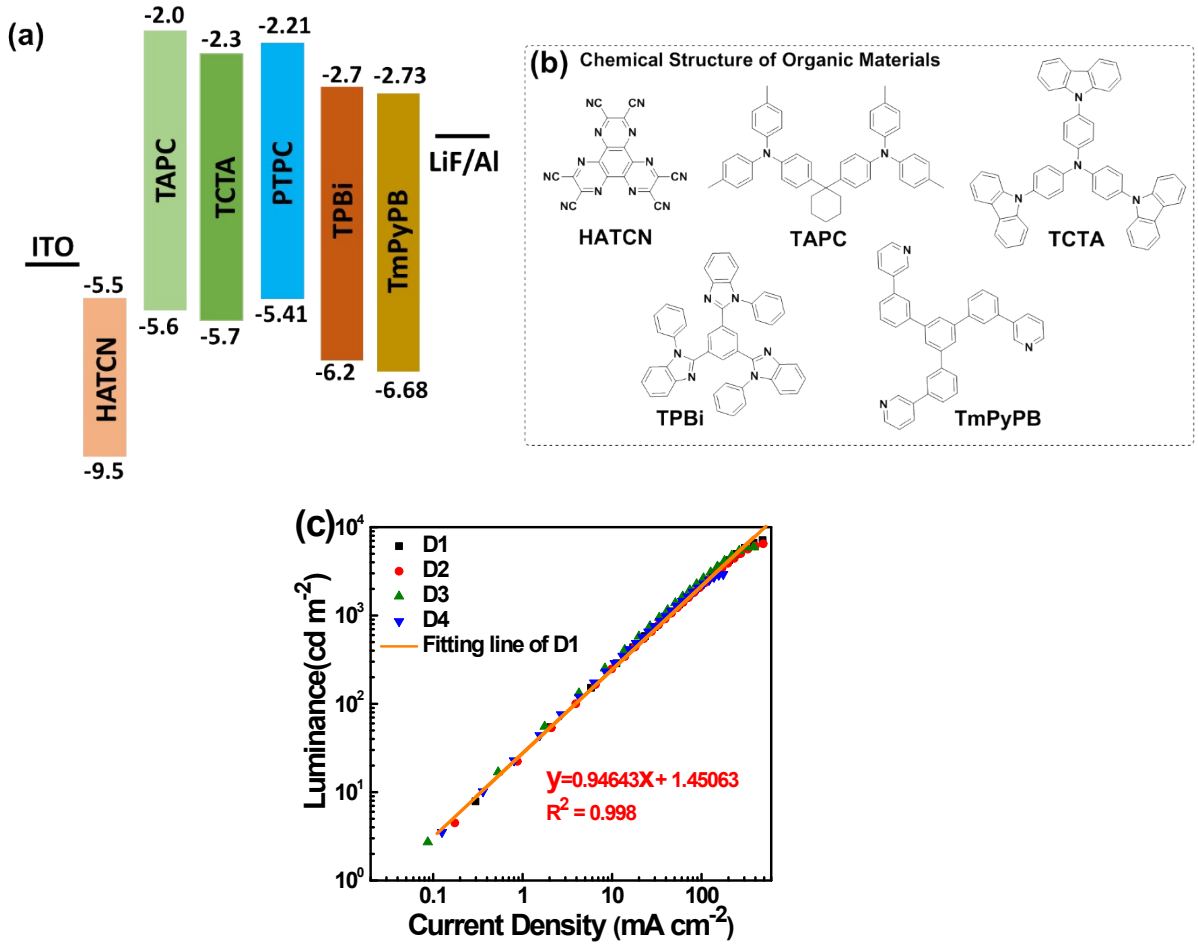

Fig. S11 The energy level alignment (a) and chemical structure of used organic materials (b) in the devices. (c) Luminance versus current density curves of the devices (**D1**, **D2**, **D3** and **D4**).

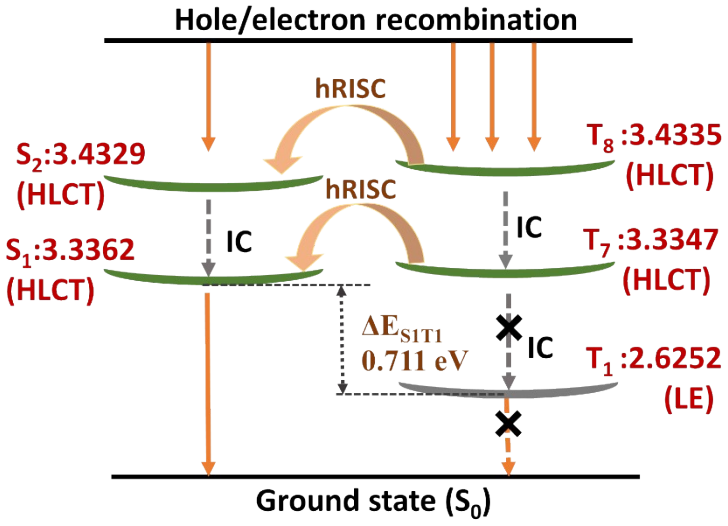

Fig. S12 Probable ‘‘hot exciton’’ mechanism caused by the HLCT states based on material **PTPC**. S: singlet state; T: triplet state; LE: local excited state; ΔE_{ST}: singlet–triplet energy splitting; IC: internal conversion; hRISC: high-lying reverse intersystem crossing.

Table S4. Summary of key EL parameters for the devices.

Devices	V_{on}[g] [V]	CE[a] max/100/1000 [cd A^{-1}]	PE[a] max/100/1000 [lm W^{-1}]	EQE[a] max/100/1000 [%]	CIE[b] (x, y)
D1	3.1	2.66/2.62/2.43	2.60/2.35/1.60	6.78/6.73/6.18	(0.156, 0.059)
D2	3.1	2.56/2.54/2.32	2.51/2.10/1.31	6.34/6.34/5.65	(0.159, 0.058)
D3	3.0	3.16/3.10/2.80	3.26/2.75/1.85	6.71/6.71/6.35	(0.158, 0.065)
D4	3.1	2.83/2.80/2.48	2.75/2.05/1.22	6.67/6.61/5.72	(0.158, 0.056)

[a] The maximum efficiencies and values taken at 100 and 1000 cd m^{-2}; [b] Measured at the voltage of 4 V; [g] At 1 cd m^{-2}.

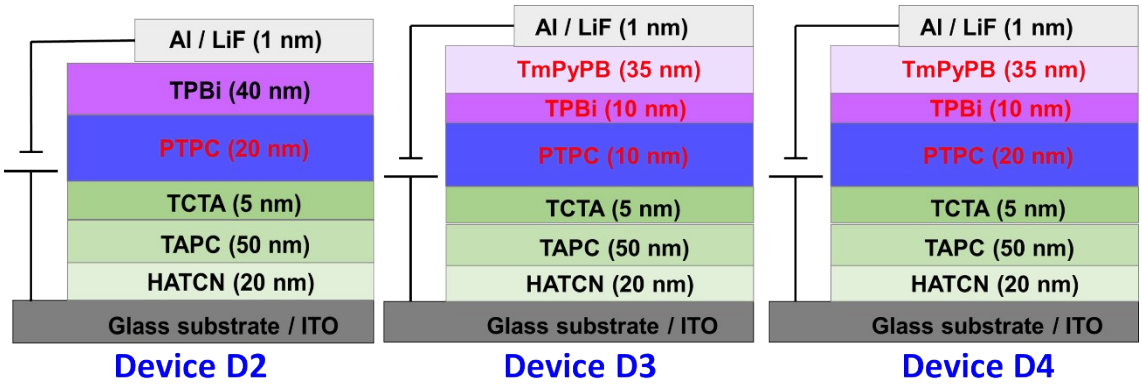

Fig. S13 Device structure diagram of the OLEDs **D2**, **D3** and **D4**.

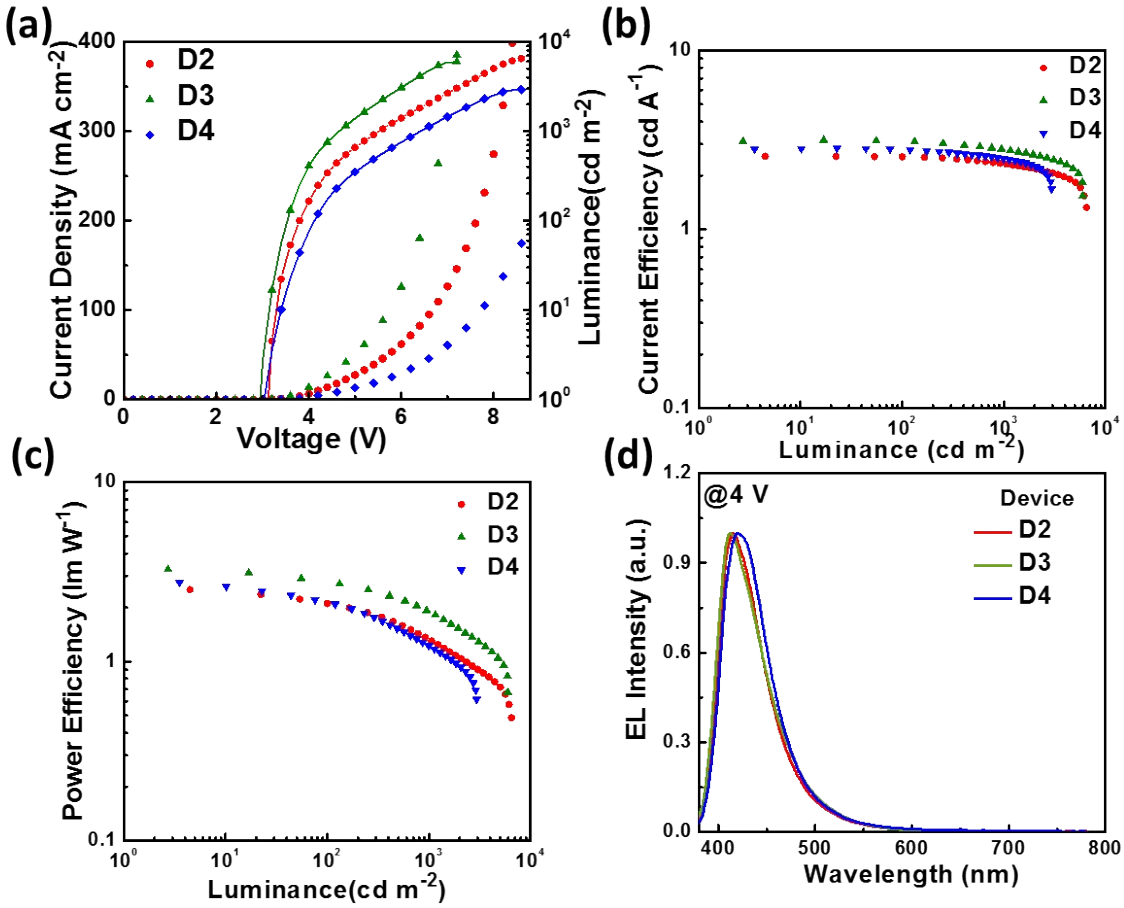

Fig. S14 (a) Current density and luminance versus voltage curves of the devices **D2**, **D3** and **D4**. (b) Current efficiency versus luminance curves of the devices **D2**, **D3** and **D4**. (c) Power efficiency versus luminance curves of the devices **D2**, **D3** and **D4**. (d) Normalized EL spectra of the devices **D2**, **D3** and **D4** at the voltage of 4 V.

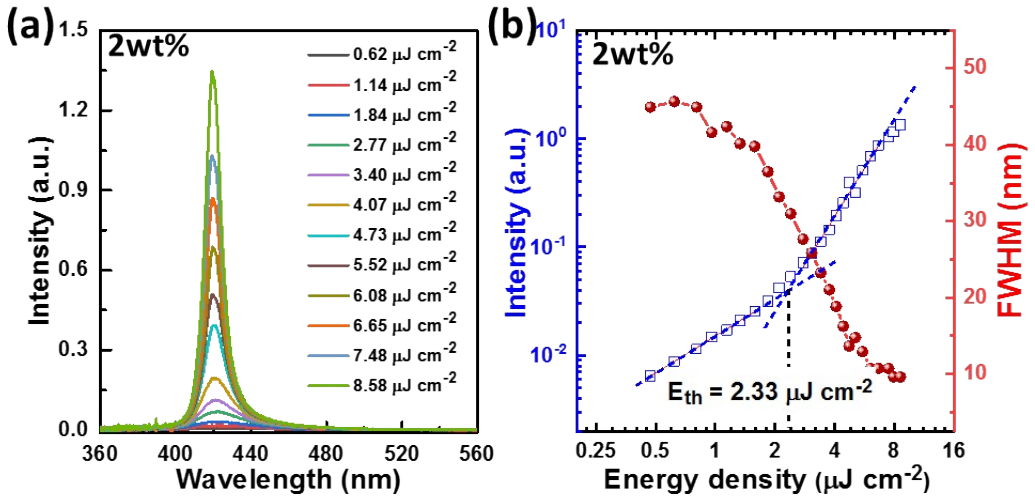

Fig. S15 (a) PL spectra of 2 wt% **PTPC** doped in mCP film at different excitation powers below and above ASE threshold. (b) PL intensity and FWHM as a function of the excitation energy of 2 wt% **PTPC** doped in mCP film.

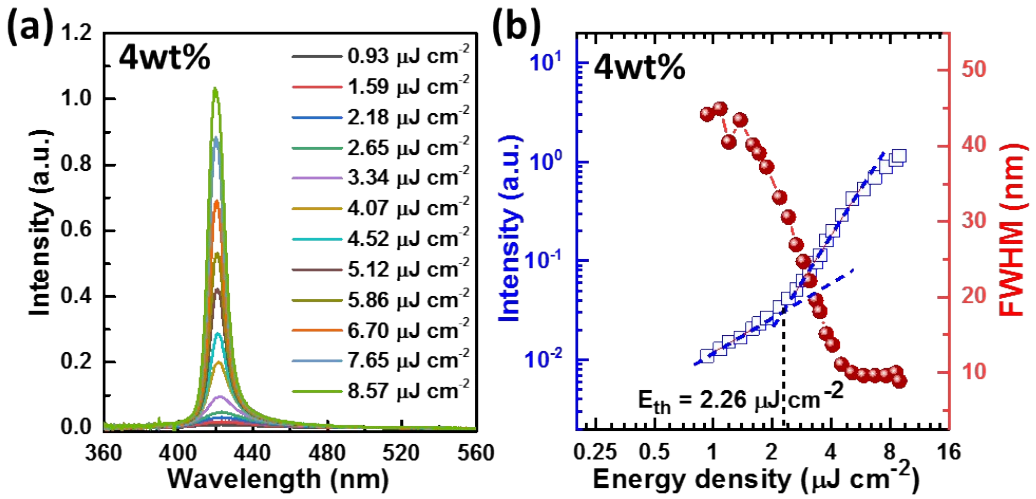

Fig. S16 (a) PL spectra of 4 wt% **PTPC** doped in mCP film at different excitation powers below and above ASE threshold. (b) PL intensity and FWHM as a function of the excitation energy of 4 wt% **PTPC** doped in mCP film.

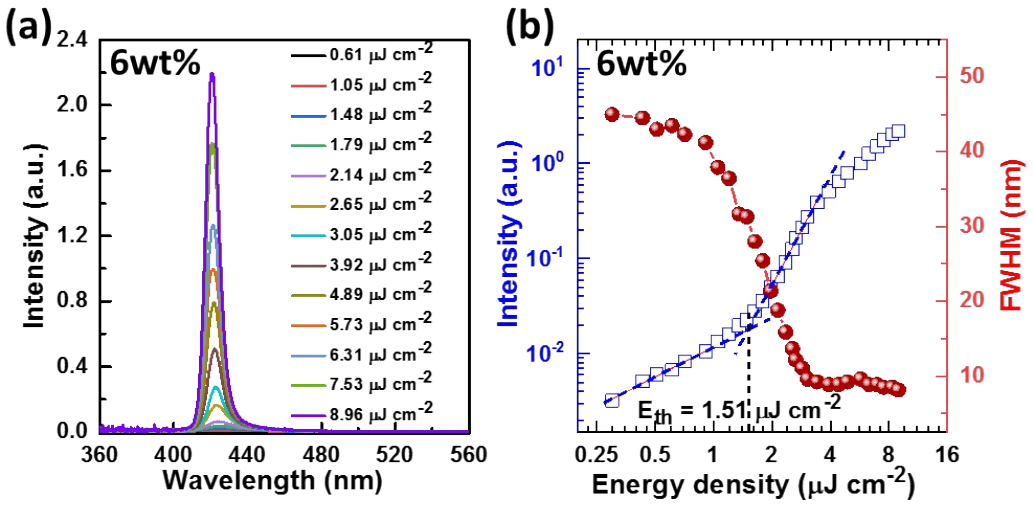

Fig. S17 (a) PL spectra of 6 wt% **PTPC** doped in mCP film at different excitation powers below and above ASE threshold. (b) PL intensity and FWHM as a function of the excitation energy of 6 wt% **PTPC** doped in mCP film.

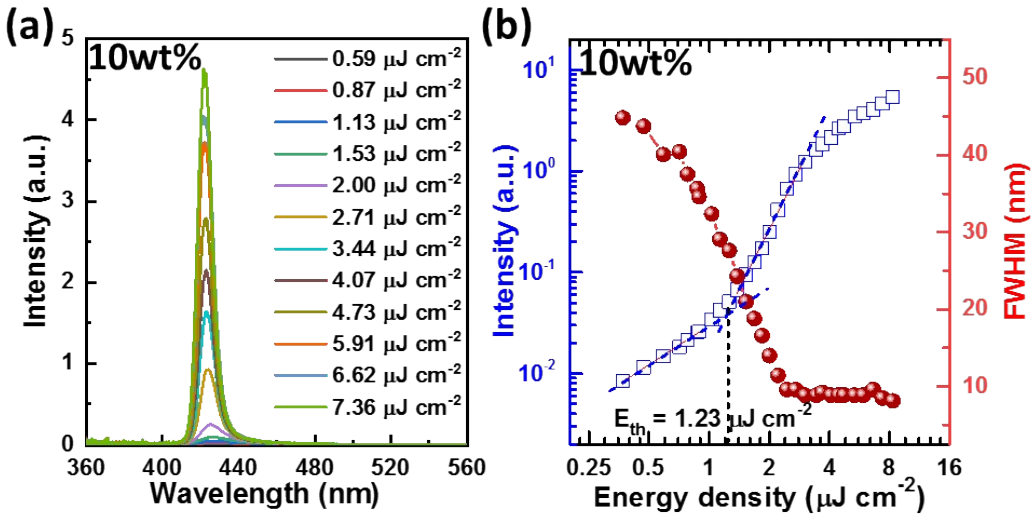

Fig. S18 (a) PL spectra of 10 wt% **PTPC** doped in mCP film at different excitation powers below and above ASE threshold. (b) PL intensity and FWHM as a function of the excitation energy of 10 wt% **PTPC** doped in mCP film.

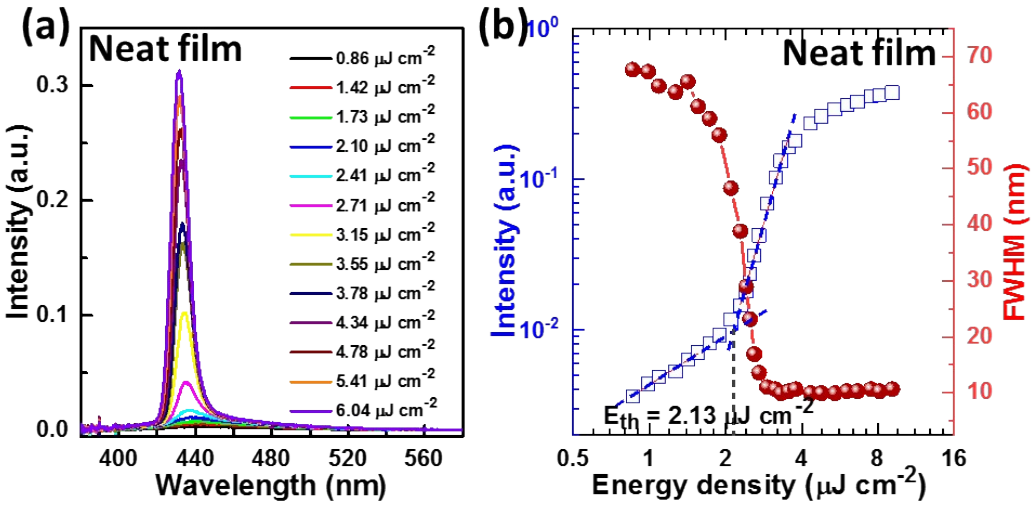

Fig. S19 (a) PL spectra of **PTPC** neat film at different excitation powers below and above ASE threshold. (b) PL intensity and FWHM as a function of the excitation energy of **PTPC** neat film.

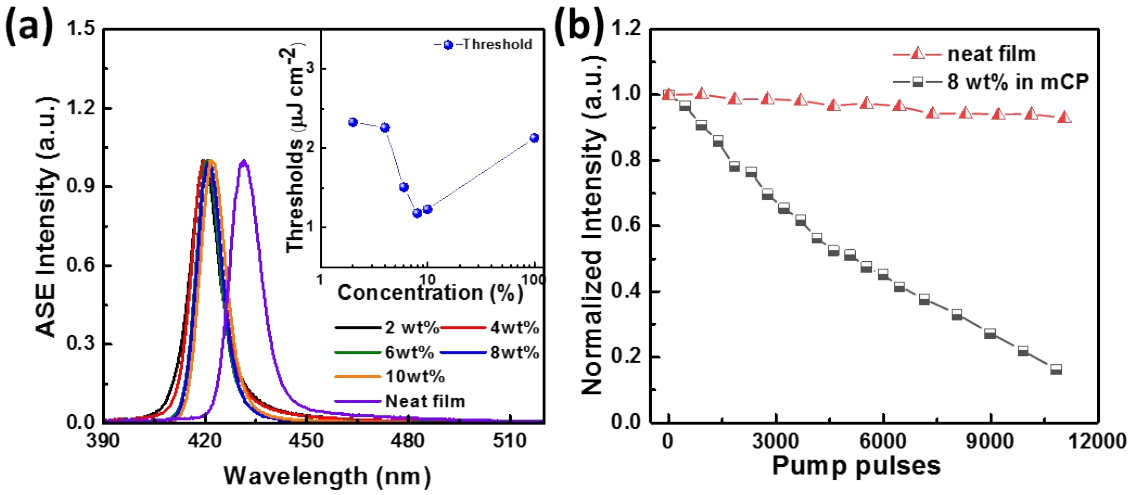

Fig. S20 (a) ASE spectra of all the films above the thresholds. The inset shows the evolution of the ASE thresholds with different doping ratios. (b) ASE intensities normalized to the initial decomposition as a function of pump pulses for neat film and 8 wt% **PTPC** doped in mCP film, irradiated by continuous-wave laser at 343 nm with the excitation intensity of 8.0 μJ cm^{-2}.

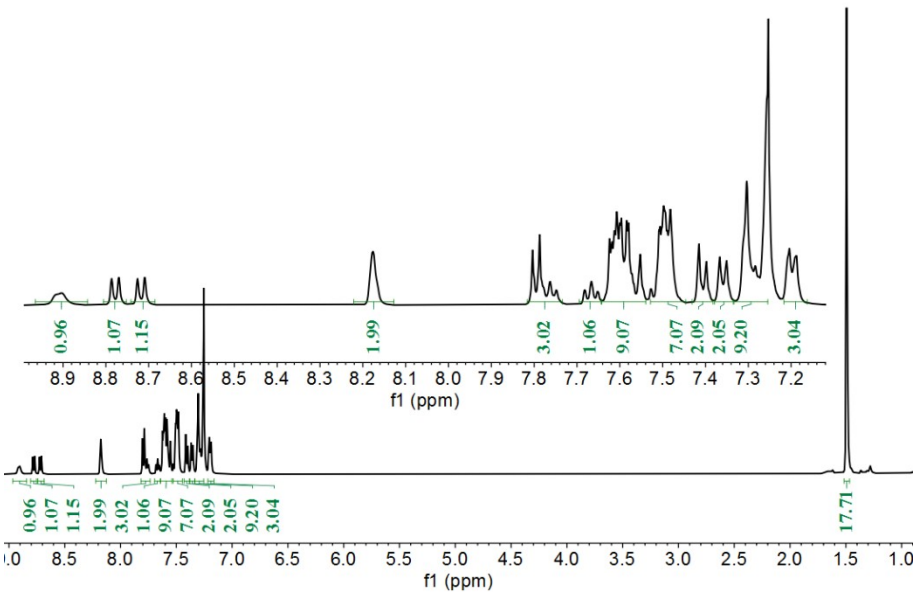

Fig. S21 [1]H NMR spectrum of the compound **PTPC**.

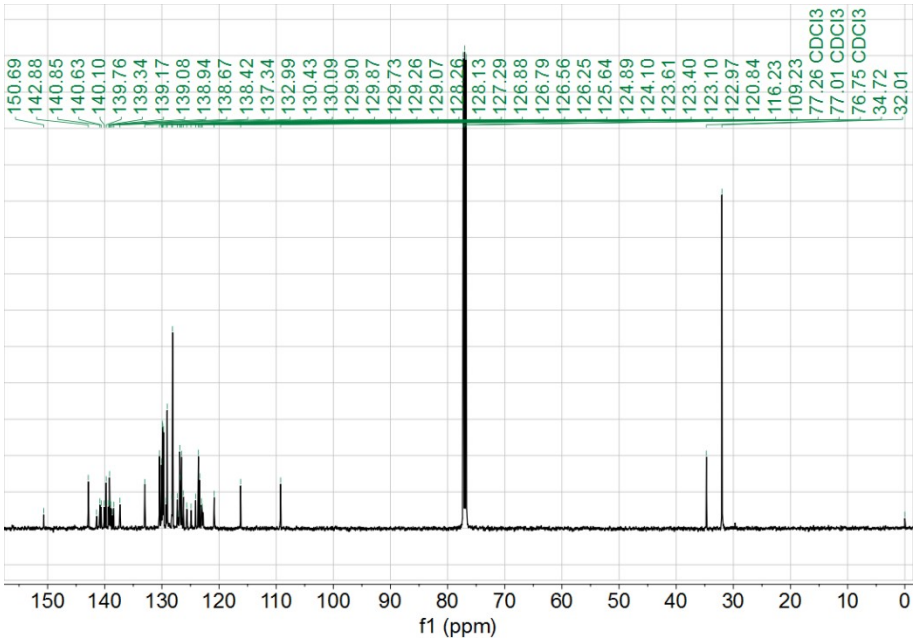

Fig. S22. [13]C NMR spectrum of the compound **PTPC**.

Reference

[1] T. Lu, F. W. Chen. Multiwfn: A multifunctional wavefunction analyzer. J. Comput. Chem., 2012, 33(5):580-92.